


Criticality in collective behavior of biogenic single-domain nanomagnetitesM. Khoddam,¹ Z. Sheidafar,¹ M. D. Nirry,^{1,2,*} and M. R. H. Khajepour¹¹*Department of Physics, Institute for Advanced Studies in Basic Sciences (IASBS), Zanjan 45137-66731, Iran*²*Center for Research in Climate Change and Global Warming (CRCC), Institute for Advanced Studies in Basic Sciences (IASBS), Zanjan 45137-66731, Iran* (Received 21 February 2018; revised manuscript received 2 August 2018; published 25 September 2018)

The origin and the functions of more than a billion single-domain magnetic nanoparticles [reported in *Proc. Natl. Acad. Sci. USA* **89**, 7683 (1992)] adjacent to billions of neurons in the brain neocortex are not known yet. There is empirical evidence implicating the sensitivity of many living organisms to constant or extremely low-frequency magnetic fields. Navigation and routing of migratory birds by the Earth's magnetic field and certain behaviors of magnetic bacteria are well-known examples. However, it seems that human beings are not able to sense the Earth's magnetic field. In this article, we first investigate the criticality of interacting magnetic superclusters in a mean-field approximation and then discuss the rotational Brownian motion of a single-domain magnetic dipole. Then, we consider the rotational Brownian motion in the presence of magnetic interactions. Ignoring the complexity of the dynamics, the anisotropy, and the long-range interaction of nanoparticles, we investigate numerically their behavior using a finite-size two-dimensional Ising-like model. It is shown that if the dipole coupling coefficient is fine-tuned to keep the model close to the critical state, then system sensitivity to an external magnetic field is maximized with an scaling behavior in terms of the number of magnetic superclusters.

DOI: [10.1103/PhysRevE.98.032133](https://doi.org/10.1103/PhysRevE.98.032133)**I. INTRODUCTION**

There are about 20 billion neurons in the human cerebral cortex, each of them having tens of thousands synapses [1]. The complexity of the functions of such a highly connected system, despite extensive research, is not yet fully understood. Since late 1980s, we also know that there exist several billions of magnetic nanoparticles in the human cerebral tissue, as well as in the other parts of central nervous system [2]. As an example, the number density of the magnetic nanoparticles in meninges is some 20 times that of the cerebral cortex. In the absence of conclusive experimental evidence, researchers have tried various hypotheses regarding the function of these nanoparticles in the brain [3]. For example, some people have advanced the idea that the magnetic nanoparticles produce a magnetic field which may play the role of a contactless catalyst in certain chemical reactions [4]. There have also been efforts to look for certain behavioral evidence that human beings can sense the magnetic field [5].

Empirical evidence indicating that many living organisms are able to detect the direction or the magnitude of the Earth's local magnetic field is rather substantial [5–7]. Depending on the precision and the sensitivity of mechanisms involved, living organisms can derive a variety of information from a magnetic field. The simplest mechanism is the magnetic compass that enables an organism to move in a certain direction, such as north or south. Organisms with this ability have a “live magnetic compass.” This is tentatively demonstrated by behavioral experiments in homing pigeons, migratory birds,

lobsters, sea turtles, elasmobranch fishes, and honeybees (see Refs. [5–7], and references cited therein). A more limited number of organisms are capable to derive “magnetic maps” of approximate geographical locations based on intensity, inclination, and declination of local magnetic field [8]. In some cases, electrophysiological records indicate that the organism should be able to measure a magnetic field as small as ~ 50 nT, which is enough to detect small quenched fluctuations in the spatial pattern of the local magnetic field intensity. This is the case with animals like sea turtles and bobolink birds. They even seem to be able to sense fine variations due to magnetic rocks in the Earth's crust [5,6].

Three main mechanisms to sense magnetic fields are recognized in living organisms: (1) electromagnetic induction, (2) response of single-domain (SD) biogenic magnetic or superparamagnetic nanoparticles (i.e., Fe_3O_4) to a magnetic field, and (3) magnetic field-dependent chemical reactions (i.e., radical pair mechanism) [5–7]. A fourth possibility is by using temporal variations in intensity of the Earth's dc magnetic field or extremely low frequency electromagnetic fields [9–11]. Our prime focus here is the modeling of systems of interacting SD biogenic magnetic nanoparticles in human brain tissue. For frequencies larger than the superparamagnetic relaxation rate, the superparamagnetic nanoparticles behave as SDs [12,13]. To make the model simpler we will not include them in our discussions. All of these mechanisms are extensively reviewed in the literature (see Refs. [5–7,14] and references cited therein).

Biogenic SD magnetic nanoparticles, which include magnetite (magnetic iron oxide, Fe_3O_4) and greigite (magnetic iron sulfide, Fe_3S_4 , for example, see Ref. [15]), are observed in body tissues of some organisms such as fish, bee, algae, and the avian as well as in the magnetotactic bacteria (in this

* Author to whom correspondence should be addressed:
m.d.nirry@iasbs.ac.ir; <http://www.iasbs.ac.ir/~m.d.nirry/>

case as chains of SDs) [16–20]. In the avian it seems that the controversial issues are finally solved in favor of the role of nanomagnetite structures in their upper beak [21]. Magnetite and greigite, originally found in rocks, display mineral magnetism. The mineral magnetites usually contain common impurities such as titanium. Moreover, mineral crystals are not usually perfect. They contain disorders such as vacancies, disclinations, and dislocations. Furthermore, their sizes are random and follow a log-normal distribution function, which means that some of them are larger than a single domain [22]. But the SD magnetic nanoparticles in the tissues of living organisms are pure and have regular crystal lattices. They are of accurate shape and uniform size (i.e., isometric). Biomagnetite crystals are also grown along the (111) crystal axis which maximizes their net magnetic moment. In addition to all the above specifications, they are small enough to include only a SD. While in a large mineral multidomain particle the random orientations of magnetic moments of different domains reduce the net magnetic moment, in living organisms a group of SD nanoparticles are aligned dipoles in a discrete supercluster (or a chain) to produce a large net magnetic moment [2,14,22]. The function of the magnetic chains has been studied in some living organisms, and at least in the case of magnetotactic bacteria this function is well understood. It is also guessed that SD nanoparticles are produced via a chemogenetic process controlled by the genomic magnetosome island in the genomic DNA of the bacteria [14].

In the human brain, both the existence of 5 million SD magnetic nanoparticles per gram of brain tissue and their function are mysteries [2]. Some research workers have guessed that they are vestigial remnants from an earlier *Homo* such as *Homo erectus* [5]. Others attribute them to airborne pollution [23]. However, the biogenic origin of magnetic particles seems to be favored [24]. The presence of biomagnetite nanoparticles in human brain tissues was first reported by Kirschvink *et al.* using transmission electron micrographs and superconducting quantum interference device [2]. In a destructive approach they froze the brain tissue in the liquid nitrogen; then they crushed this fragile tissue into very small fragments, which were then washed with distilled deionized water. The nanomagnetites were separated from the resulting solution by a fine magnetic needle. Their method is suitable for careful study of the structure of the SD nanoparticles but not for specification of the arrangement and the way the SD nanoparticles are connected in cells. Their experimental results for the human cerebral cortex shows that these nanoparticles are arranged into discrete superclusters (SCs) which are comprised of almost 100 SD nanoparticles [2]. This arrangement into superclusters is due to attractions and repulsions of tiny SD nanomagnets as well as elastic forces applied by the membrane. Nondestructive studies based on the magnetic behavior of the tissue also show that the nanoparticles inside a supercluster interact with each other [2,25]. However, until more experimental studies are available, the only way before us is to propose qualitative models based on the existing evidence.

Following other researchers, we assume that only a fraction of SD magnetic nanoparticles (or chains of SDs) are connected to the gated ion channels [11,22,26]. We try to

investigate whether the dipole-dipole interactions between superclusters are strong enough to make the system magnetically critical. In Sec. II, we examine the condition of critical coupling using the mean-field approximation. If a magnetic system is close to its critical point, then it is more susceptible to respond to changes of an applied magnetic field. Then, in Sec. III, we investigate in detail the rotational Brownian motion of noninteracting and interacting SD nanoparticles in an external magnetic field. An Ising-like model is then used to show the dynamical behavior in the critical state and estimate the sensitivity of the system to an external factor as compared to the behavior in the disordered state far from criticality. Finally, the general conclusions are presented and discussed.

II. MEAN-FIELD THEORY

The magnetic dipole-dipole coupling is a long-range anisotropic interaction. To study the dynamics of a system of magnetic dipoles, we should consider their interaction. We may have a magnetic phase for this system if the density of dipoles is greater than a certain critical value. We assume that our magnetic dipoles (the superclusters of SD nanoparticles) are more or less uniformly distributed over large-enough patches of the tissue with no frustrations and they are all of the same magnitude $\mu = N_{sc}\mu_m$ where N_{sc} is the average number of SD nanoparticles with magnetic moment μ_m in a supercluster. We also assume that the statistical fluctuations of the dipoles are homogeneous.

For two dipoles, 1 and 2, the interaction can be written as

$$U_{12}(\mathbf{r}_{12}) = \frac{-\mu_0[3(\boldsymbol{\mu}_1 \cdot \hat{\mathbf{r}}_{12})(\hat{\mathbf{r}}_{12} \cdot \boldsymbol{\mu}_2) - \boldsymbol{\mu}_1 \cdot \boldsymbol{\mu}_2]}{4\pi|\mathbf{r}_{12}|^3}, \quad (1)$$

where $\boldsymbol{\mu}_i$ ($i = 1, 2$) is magnetic moment of dipole i and \mathbf{r}_{12} is the relative position of dipoles. To write the equation in a compact form, we define the dipole-dipole coupling tensor as

$$\vec{\mathbf{J}}(\mathbf{r}) := \frac{\mu_0[3\hat{\mathbf{r}}\hat{\mathbf{r}} - \mathbb{1}]}{4\pi|\mathbf{r}|^3}, \quad (2)$$

where $\hat{\mathbf{r}}\hat{\mathbf{r}}$ represent the dyadic product $\hat{\mathbf{r}}$ and $\hat{\mathbf{r}}$ and $\mathbb{1}$ is the rank-2 unit matrix in three dimensions. Thus, Eq. (1) can be written as

$$U_{12}(\mathbf{r}_{12}) = -\boldsymbol{\mu}_1 \cdot \vec{\mathbf{J}}(\mathbf{r}_{12}) \cdot \boldsymbol{\mu}_2. \quad (3)$$

The Hamiltonian of a system of N interacting dipoles in a magnetic field \mathbf{B} can then be written as

$$H(\{\boldsymbol{\mu}_i\}) = -\frac{1}{2} \sum_{\substack{i,j=1 \\ i \neq j}}^N \boldsymbol{\mu}_i \cdot \vec{\mathbf{J}}(\mathbf{r}_{ij}) \cdot \boldsymbol{\mu}_j - \sum_{i=1}^N \boldsymbol{\mu}_i \cdot \mathbf{B}. \quad (4)$$

A. Two-dimensional case

First, we try to solve the simpler problem of dipoles uniformly distributed on the flat two-dimensional plane (arbitrary uniform lattice). Thus, \mathbf{r} is a two-dimensional vector in the plane but the dipole moments are arbitrary three-dimensional vectors. In the continuous limit, Hamiltonian [Eq. (4)] can be

written as

$$H(\{\boldsymbol{\mu}_i\}) = - \sum_{i=1}^N \boldsymbol{\mu}_i \cdot \left[\frac{\sigma_c}{2} \int_{l/2}^{\infty} \int_0^{2\pi} \tilde{\mathbf{J}}(\mathbf{r}) \cdot \boldsymbol{\mu}(\mathbf{r}) r d\varphi dr + \mathbf{B} \right],$$

by an integration over the polar coordinates. Here l is the average center-to-center distance of clusters and $\sigma_c = 4/(\pi l^2)$ the surface number density of dipoles. The lower limit of the radial integral means that an additional hard-sphere repulsive potential is assumed between superclusters which makes sure that they do not overlap [27]. Now we use a mean-field approximation by replacing $\boldsymbol{\mu}(\mathbf{r})$ with $\langle \boldsymbol{\mu} \rangle$. The Hamiltonian is then simplified as

$$H(\{\boldsymbol{\mu}_i\}) = - \sum_{i=1}^N \boldsymbol{\mu}_i \cdot (\tilde{\mathbf{J}}_{\text{eff}} \cdot \langle \boldsymbol{\mu} \rangle + \mathbf{B}), \quad (5)$$

where $\tilde{\mathbf{J}}_{\text{eff}} := (\sigma_c/2) \int_{l/2}^{\infty} \int_0^{2\pi} \tilde{\mathbf{J}}(\mathbf{r}) r d\varphi dr$. Now, one can use Eq. (2) and integrate over the polar coordinates and conclude that

$$\tilde{\mathbf{J}}_{\text{eff}} = \begin{pmatrix} \mu_0 \\ \pi l^3 \end{pmatrix} \begin{pmatrix} 1 & 0 & 0 \\ 0 & 1 & 0 \\ 0 & 0 & -2 \end{pmatrix}. \quad (6)$$

The negative value of the (3,3) component of $\tilde{\mathbf{J}}_{\text{eff}}$ indicates that the transverse component of dipole moments tend to align and fluctuate antiparallel with each other, i.e., we have a ferromagnetic (antiferromagnetic) behavior for tangential (normal) component of dipole moments. In such circumstances, lattice calculation is much easier if a kind of nonfrustrated lattice (like the honeycomb which consists of two sublattices) is selected. Then, only an effective coupling factor can be calculated numerically. The two adjacent dipoles from two sublattices are equivalent to a quadrupole. So, in computation over a finite lattice we need not to worry for the long-range effects.

In analytical calculations, we did not select any lattice for the dipoles and performed the integration over entire space by assuming that $\langle \boldsymbol{\mu} \rangle$ is uniform with no sign flip in normal component. The drawback of this approach is that it cannot include the case of negative coupling constant. Therefore, here we consider a case in which $\mathbf{B}_{\perp} = 0$ and the case with $\mathbf{B}_{\perp} \neq 0$ and $\mathbf{B}_{\parallel} = 0$ is discussed in Appendix A. So, the negative term in the (3,3) component of $\tilde{\mathbf{J}}_{\text{eff}}$ is discarded, which means the contribution of transverse component is ignored. Now, defining $\mathbf{E}(\mathbf{B}) := \tilde{\mathbf{J}}_{\text{eff}} \cdot \langle \boldsymbol{\mu} \rangle + \mathbf{B}$ in the Hamiltonian Eq. (5) and calculate the partition function,

$$Z_N = \langle e^{-\beta H(\{\boldsymbol{\mu}_i\})} \rangle = \prod_{i=1}^N \langle e^{-\beta \boldsymbol{\mu}_i \cdot \mathbf{E}(\mathbf{B})} \rangle, \quad (7)$$

where $\beta = 1/(k_B T)$ and k_B and T are the Boltzmann constant and the absolute temperature. Now, without loss of generality, one can take the z axis along \mathbf{E} and integrate over all directions and obtain

$$z := \langle e^{-\beta \boldsymbol{\mu}_i \cdot \mathbf{E}(\mathbf{B})} \rangle = \left(\frac{4\pi}{\beta \mu E} \right) \sinh(\beta \mu E), \quad (8)$$

where E represents $|\mathbf{E}(\mathbf{B})|$ and $\mu = N_{sc} \mu_m$ the magnitude of net magnetic moment $|\boldsymbol{\mu}_i|$ of a supercluster containing N_{sc} single-domain nanoparticles. We also assume that all clusters have the same number N_{sc} of SD nanoparticles. Substituting Eq. (8) in Eq. (7) we obtain the Gibbs free energy per cluster as

$$g(\mathbf{B}) = -k_B T \lim_{N \rightarrow \infty} \left(\frac{1}{N} \ln Z_N \right) = -k_B T \ln(z). \quad (9)$$

The probability of a specific orientation of $\boldsymbol{\mu}$ is $p(\boldsymbol{\mu}) = z^{-1} \exp(\beta \boldsymbol{\mu} \cdot \mathbf{E})$. Hence, $\langle \boldsymbol{\mu} \rangle$ can be written as

$$\langle \boldsymbol{\mu} \rangle = \frac{1}{z} \int_0^{\pi} d\vartheta' \int_0^{2\pi} d\varphi' \sin \vartheta' e^{\beta \boldsymbol{\mu} \cdot \mathbf{E}} \boldsymbol{\mu}. \quad (10)$$

We may write $\boldsymbol{\mu} = \mu [\sin \vartheta' (\cos \varphi' \hat{\mathbf{i}} + \sin \varphi' \hat{\mathbf{j}}) + \cos \vartheta' \hat{\mathbf{k}}]$, where $\hat{\mathbf{k}} = \hat{\mathbf{E}} = \mathbf{E}/E$. Integrating over all directions and substituting for z from Eq. (8), we obtain

$$\begin{aligned} \langle \boldsymbol{\mu} \rangle &= \left(\frac{2\pi \mu}{z} \right) \hat{\mathbf{E}} \int_0^{\pi} \cos \vartheta' \exp(\beta \mu E \cos \vartheta') \sin \vartheta' d\vartheta' \\ &= \mu [\coth(\beta \mu E) - (\beta \mu E)^{-1}] \hat{\mathbf{E}}. \end{aligned} \quad (11)$$

Vectors $\boldsymbol{\mu}$, \mathbf{B} , and $\mathbf{E}(\mathbf{B})$ can be decomposed into components normal \perp and tangential \parallel to the plane of lattice. Ordered magnetic phase is to be a nontrivial self-consistent solution of Eq. (11) in zero external magnetic field. For the longitudinal component define $x := |\langle \boldsymbol{\mu}_{\parallel} \rangle|/\mu$ and $\langle \boldsymbol{\mu}_{\perp} \rangle = 0$ then Eq. (11), yields

$$x = \coth(\tilde{\beta} x) - (\tilde{\beta} x)^{-1}, \quad (12)$$

where $\tilde{\beta} := \beta \mu^2 J_{11}$. The solution is found from graphical plot of left- and right-hand side of Eq. (12) in terms of x . From a Taylor expansion of the derivative of right-hand side of Eq. (12) around $x \approx 0$, while crossing the line $y = x$ we obtain a critical value $\tilde{\beta}_c \approx 3$. Defining a dimensionless dipole coupling constant λ as the ratio of the magnetic potential to the thermal fluctuation energy

$$\lambda := \frac{\mu_0 \mu^2}{4\pi k_B T l^3}, \quad (13)$$

we shall have the estimated critical point at $\lambda_c \approx 3/4$.

For the numerical solution of the complete problem on a honeycomb (or any other structure that consists of two triangular sublattices) see Appendix A. The estimated critical point is obtained as $\lambda_c \approx 0.91$.

B. Three-dimensional case

Three-dimensional system of interacting dipoles have been studied by a variety of approaches, mostly using some modification of the mean-field theory [27–30]. The problem is approached both as continuum models using certain orientational distribution, and as discrete lattice models. Back in 1940s Luttinger and Tisza showed that interacting point dipoles on cubic lattices order at $T = 0$ [29]. Later works indicated that orientational order may be destroyed by local fluctuations due to the randomness in positions of point dipoles, which can be checked by introducing a hard sphere radius for dipoles to suppress the divergence of interaction at

very short distance [27,28]. These works have been mainly related to the ferrofluids and dipole glasses [31].

Ferromagnetic phase transitions in a system of magnetic dipoles floating in a fluid (ferrofluid) have been studied in detail in the last decades [32]. Zhang and Widom have shown that asymmetric interactions between hard-sphere dipoles leads to zero magnetization in a spherical droplet. A nonzero total magnetization is only possible for samples with asymmetric boundary, e.g., a bipolar ellipsoid (prolate or oblate spheroid) [27]. They have also found that a ferromagnetic phase is only possible for high volume fraction of magnetic particles above the threshold value of ~ 0.3 . They predicted the coexistence of isotropic and ferromagnetic fluids for slightly lower volume fraction. Mamiya *et al.* experimentally observed the phase transition for spherical iron-nitride particles covered by surfactant layer (total diameter ~ 15 nm) in a long cylindrical shape sample. They also observed the Debye relaxation while the system was moved toward the critical point [33]. A 3D ferrofluid-like model is, however, not applicable to the case we are studying, mainly because the dipoles in ferrofluids are free to move translationally. In ferrofluid, λ_c depends functionally on the volume fraction of particles (a dimensionless measure of the density) and diverges for the volume fractions lower than the critical value [28].

In our case no translational motion is assumed for the dipoles. The dipoles are located in cells which are themselves fixed in the tissue. Thus, λ_c only depends on the dimension and the spatial arrangement of dipoles. Extending the two-dimensional model of previous section to three dimensions turns out to be more complicated than it seems at the first sight. We choose instead a hexagonal lattice model similar to that of I_h ice and solve the model numerically. For details of the model see Appendix B. The critical value $\lambda_c \approx 0.91$ is obtained. There is some evidence suggesting the existence of such an arrangement of superclusters in cortex [34]; though to the best of our knowledge no other investigation is reported.

III. ROTATIONAL BROWNIAN MOTION

As already mentioned, we assume that SD nanoparticles are located in the membranes of the nerve cells [35]. A fraction of them may be connected to gated ion channels by hair bundles, usually modeled by tiny springs. We shall discuss this point briefly later in this section. The SD nanoparticles can freely rotate around their fixed center-of-mass position. They can be considered as simple magnetic dipoles, with magnetic dipole moment μ_m .

A. Rotational dynamics of noninteracting SD nanoparticles

The stochastic rotational motion of a single SD dipole under thermal agitation can be studied in the framework of rotational Brownian motion. In other words, by comparing the energy of thermal fluctuations $k_B T$ and the magnetic energy of dipole, we can estimate the sensitivity of a single particle to the external magnetic field. The rotational Brownian motion of a magnetic dipole in a magnetic field is similar to the rotational Brownian motion of electric dipole in an electrical field. The approach to the problem and details of the calculations

are given in Ref. [36]. Here, we only give a summary of the approach.

The coupled dynamical equations for rotational Brownian motion of spherical SD nanoparticles with a magnetic dipole moment μ_m in an external magnetic field \mathbf{B} under the influence of stochastic thermal fluctuations and in a viscous medium in three dimensions are given by

$$\dot{\mu}_m(t) = \omega(t) \times \mu_m, \quad (14a)$$

$$\mathbf{I}\dot{\omega}(t) + \zeta\omega = \mathbf{w}(t) + \mu_m \times \mathbf{B}. \quad (14b)$$

Equation (14a) represents the rate of change in $\mu_m(t)$ due to the angular rotation (ω is the angular velocity). Equation (14b) is the Euler-Langevin equation of rotational Brownian motion, where $\zeta\omega$ is the damping torque due to the viscosity, $\mathbf{w}(t)$ is the thermal fluctuation torque, and $\mu_m \times \mathbf{B}$ is the torque due to an externally applied magnetic field. \mathbf{I} is the moment of inertia of the nanoparticle and $\zeta = 8\pi a^3 \eta$ is the rotational friction coefficient of a sphere with radius a that rotates in a fluid with the dynamic viscosity η . If we take the scalar product of Eq. (14a) with $\mu_m(t)$, then we find that the amplitude of the magnetic moment does not change over time. Thermal fluctuation $\mathbf{w}(t)$ is a random white noise vector with Gaussian distribution, and zero mean value $\langle \mathbf{w} \rangle = \mathbf{0}$, and its correlation function obeys

$$\langle w_i(t_1)w_j(t_2) \rangle = 2k_B T \zeta \delta_{ij} \delta(t_1 - t_2), \quad (15)$$

where $\langle \dots \rangle$ is an ensemble average and indices $i, j = 1, 2, 3$ represent the Cartesian coordinate axes.

The contribution of moment of inertia in Eq. (14b) is negligible in the low-Reynolds-number regime. Then, substituting ω in Eq. (14a) and using the triple vector product identity yield the Langevin description of the dynamics of a single-dipole in the noninertial limit as

$$\zeta \dot{\mu}_m(t) = \mathbf{w}(t) \times \mu_m(t) + \mu_m^2 \mathbf{B}(t) - [\mu_m(t) \cdot \mathbf{B}(t)] \mu_m(t).$$

The corresponding probabilistic representation through the Fokker-Planck equation can be obtained by repeating the analytical method explained in Ref. [36] as

$$2\tau_D \frac{\partial c(\vartheta, t)}{\partial t} = \frac{1}{\sin \vartheta} \frac{\partial}{\partial \vartheta} \left[\sin \vartheta \frac{\partial c}{\partial \vartheta} + \frac{\mu_m B(t)}{k_B T} (\sin^2 \vartheta c) \right]. \quad (16)$$

Equation (16) is in fact the Smoluchowski equation in spherical polar coordinates (ϑ, φ) , and $c(\vartheta, t)$ is the density of dipole moment orientations on a sphere of unit radius, and $\tau_D = 1/(2D)$ is the Debye relaxation time defined by the rotational diffusion coefficient $D = k_B T / \zeta$. Note that we have assumed a uniform external magnetic field $\mathbf{B}(t) = B(t)\hat{\mathbf{k}}$ with axial symmetry, so that $c(\vartheta, t)$ does not depend on coordinate φ in Eq. (16).

For a uniform magnetic field

$$B(t) = \begin{cases} B_0 & : t < 0 \\ 0 & : t \geq 0 \end{cases}, \quad (17)$$

i.e., $B(t) = B_0 \Theta(-t)$, where $\Theta(t)$ is the Heaviside step function. The solution of Eq. (16), can be found in linear

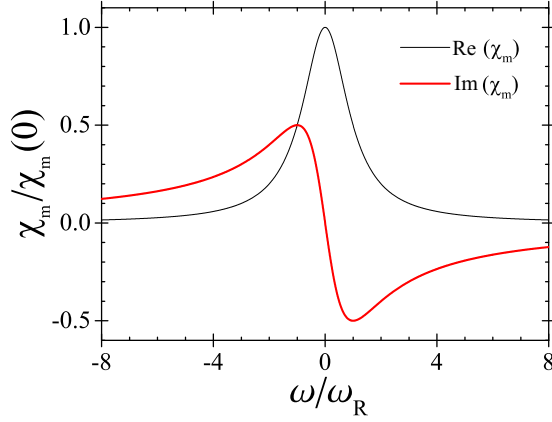


FIG. 1. Real and imaginary susceptibilities versus reduced angular frequency. The peak of absorption is at the frequency $\omega_R \sim \tau_D^{-1}$.

approximation for $\mu_m B_0 \ll k_B T$ as

$$c(\vartheta, t) = \frac{1}{4\pi} \left[1 + \left(\frac{\mu_m B_0}{k_B T} \right) e^{-t/\tau_D} \cos \vartheta \right]. \quad (18)$$

The mean magnetic dipole moment in an external magnetic field is obtained as

$$\langle \boldsymbol{\mu}_m \cdot \hat{\mathbf{k}} \rangle = \mu_m \langle \cos \vartheta \rangle = \left(\frac{\mu_m^2 B_0}{3k_B T} \right) e^{-t/\tau_D}. \quad (19)$$

If $B(t) = B_0 e^{i\omega_0 t}$ is an alternating magnetic field with angular frequency ω_0 (i.e., the alternating magnetic field is only arisen from the real part of $e^{i\omega_0 t}$), so we have

$$\langle \boldsymbol{\mu}_m(t) \cdot \hat{\mathbf{k}} \rangle = \left(\frac{\mu_m^2 B_0}{3k_B T} \right) \frac{e^{i\omega_0 t}}{1 + i\omega_0 \tau_D}, \quad (20)$$

where $e^{i\omega_0 t}$ is the temporal oscillating phase and $(1 + i\omega_0 \tau_D)^{-1}$ indicates the phase difference between the external magnetic field $B(t)$ and the magnetic moment $\boldsymbol{\mu}_m(t)$. We can write Eq. (20) as

$$\langle \boldsymbol{\mu}_m(t) \cdot \hat{\mathbf{k}} \rangle = \left(\frac{\mu_m^2 B_0}{3k_B T} \right) \left(\frac{e^{i\omega_0 t}}{1 + \omega_0^2 \tau_D^2} \right) (1 - i\omega_0 \tau_D). \quad (21)$$

Equation (21) shows that the mean magnetic dipole moment contains both real and imaginary parts. Multiplying both sides of Eq. (21) by dipole density n , and using the relation $M_z = \chi_m H_z = \chi_m B / \mu_0$, the real and the imaginary parts of magnetic susceptibility are obtained as

$$\text{Re}[\chi_m(\omega_0)] = \frac{\chi_m(0)}{1 + \omega_0^2 \tau_D^2}, \quad (22a)$$

$$\text{Im}[\chi_m(\omega_0)] = -\omega_0 \tau_D \left[\frac{\chi_m(0)}{1 + \omega_0^2 \tau_D^2} \right], \quad (22b)$$

where $\chi_m(0) = \mu_m^2 \mu_0 n / (3k_B T)$ and μ_0 is the magnetic constant. The imaginary part of the magnetic susceptibility indicates the energy absorption from electromagnetic field by the magnetic nanoparticles (Fig. 1).

According to the Eq. (22b) the maximum energy absorption from electromagnetic field occurs at angular frequency $\omega_R = 1/\tau_D$, which is called the resonant frequency. Using the

definition of the Debye relaxation time we obtain

$$\omega_R = 2k_B T / \zeta = \frac{k_B T}{4\pi \eta a^3}. \quad (23)$$

The elastic effects mentioned earlier are investigated in detail in the literature [11,22,26]. The hair bundle (spring) stiffness k which normally shuts the gated ion channel is ignored in our calculations. A simple calculation shows that the corresponding elastic energy is the smallest term. For a small displacement of hair bundle in a time scale larger than millisecond the stiffness k is $\approx 250 \mu\text{N/m}$ [35]. The gated ion channel is opened by a displacement of about $\delta \approx 4 \text{ nm}$ [11,22]. Thus, the dimensionless number λ' which represents the ratio of the elastic potential energy to thermal fluctuation can be estimated as $\frac{1}{2} f k \delta^2 / (k_B T) \approx 0.4 f$, where $f \ll 1$ shows the fraction of SD nanoparticles which are connected to the gated ion channels [12]. We should note also that most of SD nanoparticles are located in the astrocytes rather than nerve cells [23,24,34,37]. Therefore, the contribution of hair bundle elasticity is at least an order of magnitude less than other terms.

All of our calculation in this section is performed for monodisperse nanoparticles. To extend the results to polydisperse nanoparticles, one should take average of Eq. (22b) over the size distribution:

$$\left\langle \left| \frac{\text{Im}[\chi_m(\omega_0)]}{\chi_m(0)} \right| \right\rangle_a = \left(\frac{\omega_0}{\omega_R} \right) \left\langle \frac{(a/\bar{a})^3}{1 + (\omega_0/\omega_R)^2 (a/\bar{a})^6} \right\rangle_a. \quad (24)$$

B. Rotational dynamics of interacting SD nanoparticles in a supercluster

We will later discuss that the distance of SD nanoparticles in a supercluster are about a few micrometers and the energy of their magnetic interaction and thermal fluctuation are comparable. The magnetic field acting on a SD nanoparticle is the sum of the external magnetic field and the net magnetic field resulting from other SD nanoparticles in the supercluster. In mean-field approximation, $\mathbf{E}(\mathbf{B}) = \mathbf{B} + \vec{\mathbf{J}}_{\text{eff}} \cdot \langle \boldsymbol{\mu}_m \rangle$. We consider the situation that $\mathbf{B} = B \hat{\mathbf{k}}$ and the rotation axis remains unchanged along the z axis. Based on the previous result in the supercritical state, in a nonzero magnetic field the average dipole moment $\langle \boldsymbol{\mu}_m \rangle$ is along the z axis. Therefore, $\langle \boldsymbol{\mu}_m \rangle = \mu_m \langle \cos \vartheta \rangle \hat{\mathbf{k}} = \langle \boldsymbol{\mu}_m \cdot \hat{\mathbf{k}} \rangle \hat{\mathbf{k}}$. Thus, for a symmetric $\vec{\mathbf{J}}_{\text{eff}}$, as in Eq. (6), we can write

$$\mathbf{E}(\mathbf{B}) = (B + J_0 \langle \boldsymbol{\mu}_m \cdot \hat{\mathbf{k}} \rangle) \hat{\mathbf{k}}, \quad (25)$$

where $J_0 \sim \mu_0 / (\pi l_m^3)$ and l_m is the average center-to-center distance of SD nanoparticle in a supercluster. Our previous approach is still working. However, we have to realize that our approach is linear in the $\mu_m E / (k_B T)$ (i.e., far from the critical state where $\mu_m E \sim k_B T$). Assuming a harmonic variation $e^{i\omega_0 t}$ for external magnetic field, we have

$$\mathbf{E}(\mathbf{B}, t) = E_0(B_0, \omega_0) e^{i\omega_0 t} \hat{\mathbf{k}} = [B_0 e^{i\omega_0 t} + J_0 \langle \boldsymbol{\mu}(t) \cdot \hat{\mathbf{k}} \rangle] \hat{\mathbf{k}}, \quad (26)$$

where B_0 and E_0 are complex values and B_0 may not be in phase with E_0 . To avoid repeating, we substitute $E_0 e^{i\omega_0 t}$ with $B_0 e^{i\omega_0 t}$ in Eq. (20). Then, the average dipole moment is

obtained as

$$\langle \boldsymbol{\mu}_m(t) \cdot \hat{\mathbf{k}} \rangle = \left(\frac{\mu_m^2}{3k_B T} \right) \frac{B_0 e^{i\omega_0 t} + J_0 \langle \boldsymbol{\mu}(t) \cdot \hat{\mathbf{k}} \rangle}{1 + i\omega_0 \tau_D}. \quad (27)$$

Next, with some simplification

$$\langle \boldsymbol{\mu}_m(t) \cdot \hat{\mathbf{k}} \rangle = B_0 e^{i\omega_0 t} \left(\frac{\mu_m^2}{3k_B T} \right) / (1 - \lambda_m + i\omega_0 \tau_D), \quad (28)$$

where $\lambda_m = J_0 \mu_m^2 / (3k_B T)$. As in the previous section, we can write Eq. (28) as

$$\langle \boldsymbol{\mu}_m(t) \cdot \hat{\mathbf{k}} \rangle = \frac{B_0 \lambda_m e^{i\omega_0 t} (1 - \lambda_m - i\omega_0 \tau_D)}{J_0 (1 - \lambda_m)^2 [1 + \omega_0^2 \tau_D^2 / (1 - \lambda_m)^2]}. \quad (29)$$

Finally, it can be concluded that the resonance frequency ω_R is $(1 - \lambda_m) / \tau_D$. Our calculations have been performed for $\mu_m E_0 \ll k_B T$ or equivalently $\lambda_m \ll 1$, but as expected the interaction causes a shift in the resonance frequency.

Astrocyte cell body spans 10 to 20 μm . Some of them may contain a supercluster (i.e., N_{sc} nanoparticles). Assuming a uniform distribution of SD nanoparticles in cell membrane, we would have $l_m = 4 \mu\text{m}$ and $\lambda_m \sim 1$.

IV. ISING LIKE MODEL

An old proposal exists that ‘‘a neurological array averaging over large numbers of organelles . . . would be necessary to explain the sensitivity to weak geomagnetic intensity fluctuations displayed by many animals’’ [12]. We want to show how the magnetic critical state of the receptors (i.e., magnetic superclusters in organelles) may enhance the above sensitivity beyond the usual neurological array averaging. To do so, we use the well-known Ising model which is conventionally utilized in the discussions of phase transitions in the magnetic materials. Here a dichotomic variable $s_i = \pm 1$ called spin represents the magnetic moment of site i . Neighboring spins on the lattice are coupled to each other with a constant coupling J . We use the model here to investigate the dynamics of magnetic nanoparticles. So we simplify the complexity of anisotropic long-range dipole-dipole interaction to an Ising nearest-neighbor interaction, and the magnetic dipoles are simplified to have either ‘‘up’’ or ‘‘down’’ direction.

The Ising model in an external magnetic field h is described by the Hamiltonian

$$H(\{s_i\}) = -J \sum_{[i,j]} s_i s_j - h \sum_i s_i, \quad (30)$$

where the square bracket $[i, j]$ indicates that the summation is taken over all nearest-neighbor sites.

The order parameter is magnetization M per particle and is defined as

$$m := \frac{M}{N} = \frac{1}{N} \sum_{i=1}^N s_i. \quad (31)$$

At the critical point $m \rightarrow 0$ for $h = 0$. Well above the critical point, the dynamics of the system is governed by thermal fluctuations, and dipoles are not correlated, i.e., we have a paramagnetic regime. The system is linearly sensitive to an applied magnetic field. As the critical point is approached, the

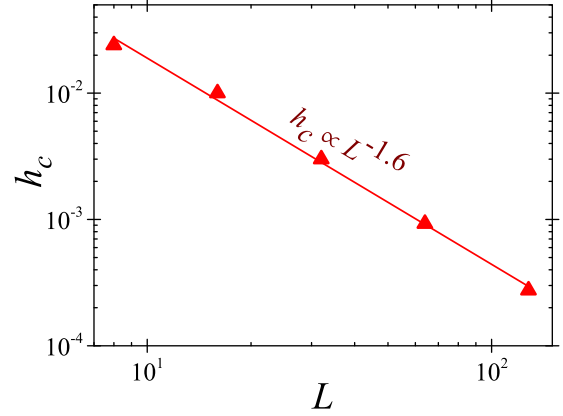


FIG. 2. The minimum external magnetic field, which causes a symmetry breaking along the external field, in terms of system size L .

correlations scale with the system size as a power law, and the susceptibility diverges.

Here we study the dynamics of a two-dimensional Ising model using a Monte Carlo simulation on a regular 128×128 lattice. In the thermodynamic limit, if the temperature of the system decreases slowly from above the critical point to below it, then the spins will align in even a tiny external magnetic field. But at finite size the external magnetic field should be greater than a threshold h_c for the spins to align. This threshold is strongly dependent on the system size L (i.e., $\lim_{L \rightarrow \infty} h_c = 0$). So, the value of h_c is a measure of sensitivity of finite Ising lattice to an external magnetic field. Our simulation shows that h_c has a power-law behavior with L when $L = 2^n$ varies from 2^3 to 2^7 (Fig. 2). For N independent particles the accuracy of mean value will vary as $N^{-0.5}$. But Fig. 2 shows that if the interaction is set at the critical point value, the accuracy will scale as $N^{-0.8}$ for an $L \times L (= N)$ lattice. This difference in the exponent is dramatically large for our model of interacting magnetic superclusters. Here the total number of superclusters in the human brain is $N \sim 10^7$ and the sensitivity might increase at least 100-fold compared to that of the noninteracting case.

A. Alternating magnetic field

The previous result presented in Fig. 2 is also valid for a very low frequency external alternating magnetic field, $h(t) = h_0 \cos(\omega_0 t)$. The Monte Carlo simulation is used in the equilibrium state with no temporal variation. But if the relaxation time scale is much smaller than the time scale of temporal variation of the external magnetic field, we may assume that the system is in the equilibrium state at each time step. A Monte Carlo simulation is used to reach the equilibrium in each time step [38]. We use this approximation for an extremely low frequency external magnetic field (i.e., frequency $\lesssim 10$ Hz).

Now, we assume the system to be at the critical point and expose it to an alternating external magnetic field, $h(t) = h_0 \cos \omega_0 t$ (the relaxation time scale $\tau \ll 2\pi/\omega_0$). Averaging over the number of Monte Carlo steps we can estimate $m(t)$ corresponding to h at time t . If the system is sensitive to $h(t)$,

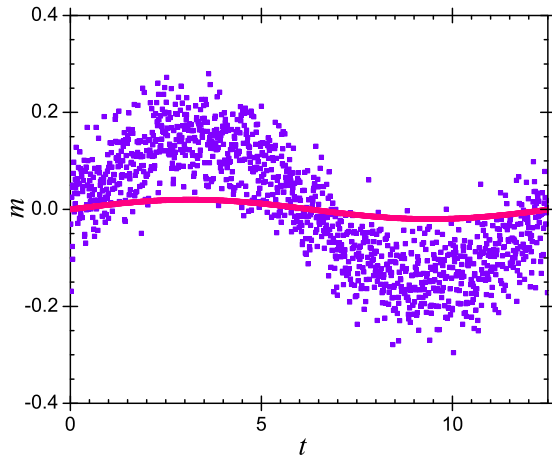


FIG. 3. The temporal variation of magnetization $m(t)$. Solid curve shows the magnetic field $h(t)$.

magnetization $m(t)$ should follow its changes (Fig. 3), and we expect a linear relationship between them [$m(t) \simeq \chi h(t)$ as in Fig. 4]. But if $h_0 < h_c$, the error (thermal fluctuation) dominates and the linear relationship between $h(t)$ and $m(t)$ will be removed. The simplest way to measure the degree of linear dependence between $m(t)$ and $h(t)$ is by plotting the Pearson's regression coefficient [39]

$$r(m, h) = \frac{\langle m(t)h(t) \rangle_t - \langle m(t) \rangle_t \langle h(t) \rangle_t}{\sigma(m)\sigma(h)}, \quad (32)$$

as a function of alternating magnetic field (Fig. 5). In Eq. (32) the symbol $\langle \dots \rangle_t$ signifies the time average, $\sigma^2(x) = \langle x^2(t) \rangle_t - \langle x(t) \rangle_t^2$ is the variance, and x represents m or h . If the Pearson's regression $r(m, h)$ is close to 1, then the magnetization follows linearly the changes of the external magnetic field, i.e., the system senses $h(t)$. The inset in Fig. 5 shows the relative error in χ versus h_0 . If the relative error is large, then dependence of the magnetization on external field is weak. In Fig. 5, $r(m, h)$ reaches the value 1.0 at an amplitude of about $h_0 \approx 10^{-2}$ and the relative error in χ decreases to its minimum value at $h_0 \approx 10^{-2}$ as shown in the inset.

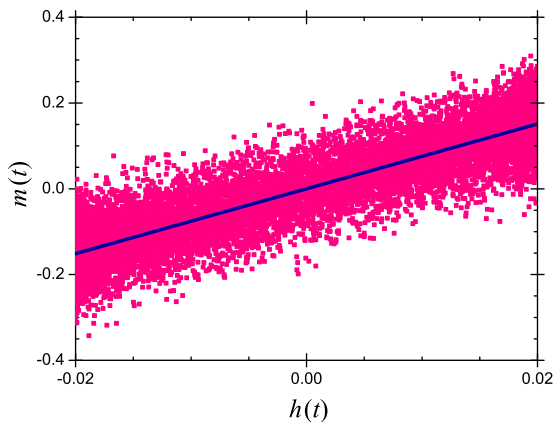


FIG. 4. A parametric plot of the magnetization $m(t)$ versus $h(t)$ (changing parameter is time). Solid line shows the linear fit to the plot of the magnetization versus h . Slope of the solid line is χ .

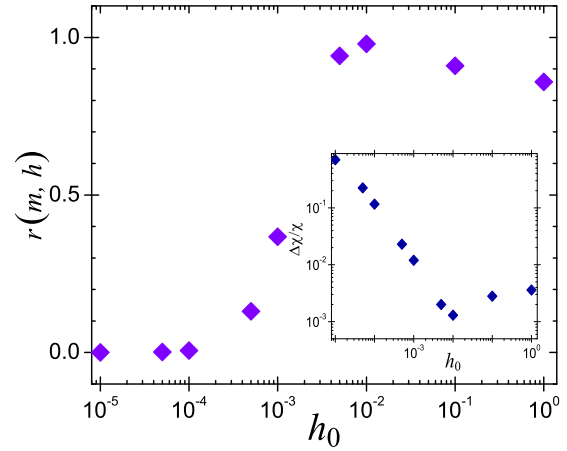


FIG. 5. The Pearson's regression coefficient for the linear relation $m(t) \simeq \chi h(t)$ as a function of amplitude of $h(t)$. (inset) Relative error of slope χ versus h_0 .

B. Spectral density

We saw that taking average over an array of receptors increase the sensitivity of system. For an oscillating signal, the averaging can be performed over time. Paulin has suggested that the nervous system can adapt itself with an oscillating external field which is sensed by all the receptors and act as a band-pass filter to remove the background noise from the periodic signals and improve the sensitivity [40]. Here, we apply fast Fourier transform to $m(t)$ and find its spectral density and look for a specific frequency in magnetization which is induced by the alternating external field (Fig. 6). To plot the spectral density we use a time series which includes at most 10 oscillations of the alternating external field (e.g., in Fig. 6, a peak at ~ 10 Hz frequency is distinguishable in a time series with length ~ 1 s).

The spectral density of the magnetization for an alternating external magnetic field with amplitude $h_0 = 5 \times 10^{-5}$ shows that its peak is much lower than the threshold in the constant magnetic field, $h_c \simeq 9 \times 10^{-4}$ (Fig. 2). Minimum detectable

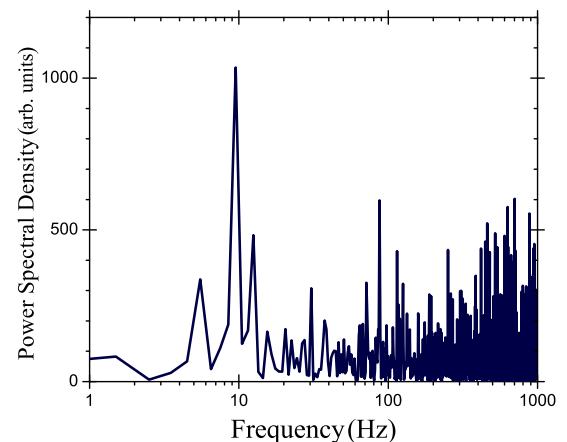


FIG. 6. Power spectral density of magnetization for the 64×64 Ising model interacts with an external sinusoidal alternating magnetic field with the amplitude of $h_0 = 5 \times 10^{-5}$ and frequency of 10 Hz.

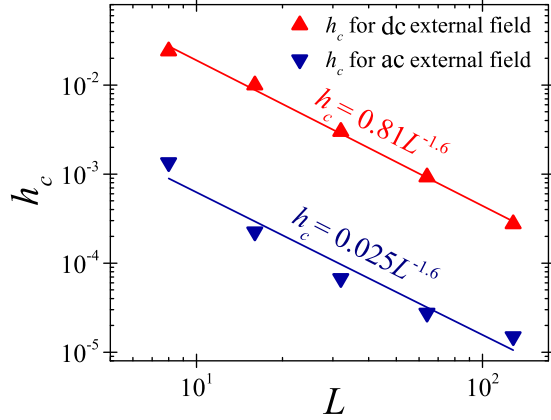


FIG. 7. The amplitude of minimum detectable external magnetic field vs. lattice size L . Solid triangle pointing upward (\blacktriangle) is the minimum constant field influences the transition. Solid triangle pointing downward (\blacktriangledown) is the minimum amplitude of alternating field that may be detected by using power spectrum of magnetization.

value by this method is shown by the solid triangles pointing downward in Fig. 7. In the figure the sensitivity to the constant and the alternating external magnetic fields are compared. Implications of this idea of improving sensitivity for nervous system are discussed by Paulin and we refer the reader to his work [40].

In summary, if the minimum measurable value of magnetization is M_{\min} , then the minimum detectable magnetic field h_c at critical point (where magnetic susceptibility diverges) is given by

$$h_c = \chi^{-1} M_{\min}, \quad (33)$$

where h_c follows power-law behavior $\propto N^{-\alpha_h}$. For a finite Ising lattice, the susceptibility at the critical point is given by [41]

$$\chi_L \propto L^{\gamma/\nu}, \quad (34)$$

where γ is the exponent of zero field susceptibility at critical point and ν is the exponent of correlation length. Since, $N = L^2$ then $h_c \propto N^{-\gamma/(2\nu)}$ and $\alpha_h = \gamma/(2\nu)$. Using the numerical values of exponents γ and ν we would then have $\alpha_h \approx 0.87$ and 0.66 for the Ising model in two and three dimensions, respectively [41]. These results confirm our numerical estimation $\alpha_h = 0.8$ in two dimension. However, these results, obtained for an Ising-like model, is not necessarily applicable to systems with dipole-dipole interaction.

V. DISCUSSIONS AND CONCLUSIONS

We have shown (Sec. II) that a system of magnetic dipoles interacting via dipole-dipole interaction exhibits a magnetically ordered phase below a temperature T if the number density of dipoles is more than a certain value. By introducing a dimensionless dipole coupling constant $\lambda := \mu_0 \mu^2 / (4\pi k_B T l_{sc}^3)$, and applying a simple mean-field approximation, we found that the critical transition point corresponds to $\lambda_c \approx 0.75$ for a two-dimensional system and to $\lambda_c \approx 0.91$ for a three-dimensional one.

Applying the above results to a system of magnetic superclusters in brain, the dimensionless dipole coupling constant is given by

$$\lambda = \frac{\mu_0 N_{sc}^2 \mu_m^2}{4\pi k_B T l_{sc}^3},$$

where l_{sc} is the average distance between clusters and N_{sc} is the average number of SD particles in a supercluster. The numerical estimates of all the parameters based on existing experimental results are given in Appendix C.

The two tissues of interest here, the neocortex and meninges, are different from each other regarding the distribution and density of superclusters. Distribution of magnetic superclusters in meninges is fairly uniform in large scale, while these superclusters are quite heterogeneously distributed in the neocortex. Also, the number density of magnetites in the meninges is an order of magnitude higher than in the neocortex. The density of magnetic nanoparticles in hippocampus is also found to be high and comparable to that in the meninges [42]. For meninges, using the estimates of Appendix C, at the body temperature $k_B T$ is $\sim 4.3 \times 10^{-21}$ J, we have $\lambda^{(\text{men})} \sim 0.7 \pm 0.3$, within the ranges of λ_c . Overall heterogeneity of distribution of magnetic particles in cortex means that cortical tissue may attain critical density in large enough patches of the tissue [2]. In some of these patches the average distance between superclusters are less than $100 \mu\text{m}$. If compared with our overall estimation in Appendix C, $l_{sc}^{(\text{cor})} \sim 3 \times 10^2 \mu\text{m}$, the density of superclusters in these patches are an order of magnitude higher than their average density in the neocortex. For these patches $\lambda^{(\text{cor})} \sim \lambda_c$. In fact, there are some evidence confirming that the superclusters are more or less uniformly distributed over these large patches [37]. Also, proximity of them to meninges tissue may critically couple them together. Open magnetic hysteresis loops observed at room temperature for the brain tumor (meningiomas) with high magnetites number density may have some relevance to our expectation [43]. Finally, it should be noted again that what we mean by criticality is different from the criticality observed in the electrocorticographic records of the cortical avalanches.

As mentioned earlier, SD nanomagnetites are organized in the groups of almost 100 SD nanoparticles (i.e., superclusters) but not in solid chains or magnetosomes. So they can rotate mechanically independent of each other in the supercluster. To investigate the rotational Brownian motion, it is more realistic to use average SD nanoparticle size instead of supercluster size in estimating the resistance due to viscosity. The average resonance angular frequency is given by Eq. (23) i.e., $\omega_R = k_B T / (4\pi \eta \bar{a}^3)$. The cell cytoplasm dynamic viscosity is about 0.1 Pa s . Using \bar{a} (as estimated in Appendix C), we estimate $\omega_R \approx 30 \text{ rad/s}$ for monodisperse particles. To extend the results to polydisperse SD nanoparticles, one may use the parameters given by Appendix C in Eq. (24) and find a broad range of resonance frequencies from 10 to 50 Hz. Also, for interacting SD nanoparticles in disordered phase far from equilibrium, we show that the resonance frequency indicates a shift, $\omega_R = (1 - \lambda_m) / \tau_D$, but close to the critical point ω_R will be a more complicated function of λ_m .

It is obvious that above results are obtained by making many simplifications (such as assuming spherical particles,

ignoring the elasticity of the involved subcellular structures, and ignoring the possible effects of the existing superparamagnetic particles). Moreover, T_c is generally overestimated in mean-field approximations. Thus, λ_c might be underestimated in our case. What is emerging from our results is that the assumption of near critical dynamics of magnetic nanoparticles in the brain tissue (or in some regions of it) is a plausible one. We have estimated the parameters of our model mostly from the pioneering experimental works of three decades ago. New and more accurate experimental data are needed to develop a better understanding of the problems and to devise more realistic models.

A system of superclusters in critical point is more sensitive to external factors, than in disordered phase. At critical point sensitivity scales with the number of superclusters as a power law $\sim N^{-\alpha_h}$; $0.5 < \alpha_h \sim 0.8$, where $\alpha_h = 0.5$ is the exponent for independent receptors. Our simple Ising-like calculations shows that the sensitivity of a system of N superclusters (as magnetic receptors) increases enormously in critical state compared to disordered state, if N is sufficiently large. Of course, we know that the Ising-like model is not a good substitute for a system of interacting dipoles.

ACKNOWLEDGMENTS

The authors thank Alireza Valizadeh for fruitful discussions. This work was supported by Institute for Advanced Studies in Basic Sciences (Grant No. G2017IASBS12644).

M.K. and Z.S. contributed equally to this work.

APPENDIX A: MEAN-FIELD THEORY OF THE HONEYCOMB LATTICE

Following the calculations in Sec. II B, here we investigate a more general problem that also allows an antiferromagnetic phase to occur. The honeycomb lattice consists of two triangular sublattices A and B. We can assume

$$\langle \mu_i \rangle = \begin{cases} \langle \mu \rangle & : i \in A \\ \mathbf{A}_r \langle \mu \rangle & : i \in B \end{cases}, \quad (\text{A1})$$

where \mathbf{A}_r is three-dimensional reflection matrix along the normal component as

$$\mathbf{A}_r = \begin{pmatrix} 1 & 0 & 0 \\ 0 & 1 & 0 \\ 0 & 0 & -1 \end{pmatrix}. \quad (\text{A2})$$

Then, we do not ignore the contribution of the normal component and $\vec{\mathbf{J}}_{\text{eff}}$ is calculated as

$$\vec{\mathbf{J}}_{\text{eff}} \approx \vec{\mathbf{J}}_{\text{eff}}(\mathbf{r}_i) = \frac{1}{2} \sum_j \vec{\mathbf{J}}(\mathbf{r}_j - \mathbf{r}_i) \mathbf{A}_j, \quad (\text{A3})$$

where \mathbf{r}_i is an arbitrary location at a center of lattice. Also, $\mathbf{A}_j = \mathbb{1}$ for $j \in A$ and $\mathbf{A}_j = \mathbf{A}_r$ for $j \in B$. Finally, $\vec{\mathbf{J}}_{\text{eff}}$ is numerically obtained from $L \rightarrow \infty$ asymptotic behavior. The critical point is estimated at $\lambda_c \approx 0.91$ (1.29) for the ferromagnetic (antiferromagnetic) phase based on the tangential (normal) component of $\langle \mu \rangle$. Therefore, with increase in λ (i.e., the dipoles density), we expect that the ferromagnetic phase appears first and the other one is meaningless. However,

the values of these two λ_c are estimated to be close together. Thus, more accurate calculations may shift them relative to each other rather than the mean-field approximation in favor of antiferromagnetic phase.

APPENDIX B: MEAN-FIELD THEORY OF THREE-DIMENSIONAL CASE

A model that provides us with the kind of three-dimensional structure compatible with the dipole-dipole interaction is that of I_h ice. In ice I_h the electric dipoles are on the vertices of a tetrahedron whose center (oxygen atom) lies on a hexagonal lattice, so that in each tetrahedron two of the dipoles are oriented inward and the remaining ones are oriented outward. Hexagonal lattice consists of two triangular sublattices A and B. Base of all tetrahedrons tangentially lie down on hexagonal planes. But apices of tetrahedrons whose centers are on the two sublattices are oppositely oriented [44].

Similarly, we arrange the magnetic dipoles on the vertices of a tetrahedron [Fig. 8(a)]. Then, the center of half of tetrahedrons are laid on the sublattice A (B), while their apices above (below) the planes of hexagonal lattice. Stack of planes coupled to each other by the dipoles at the apices of tetrahedrons. We should analyze the structure produced [Fig. 8(b)], and find effective coupling between dipoles. In this case, thermal fluctuations of all dipoles will not be around a fixed orientation. Rather, it is assumed that each dipole fluctuates on average along a segment of the line from the tetrahedron's centroid to the corresponding vertex [i.e., along the directions of OA, BO, OC, or DO in Fig. 8(a)]. Therefore, instead of the simple reflection matrix at Eq. (A2) five distinct orthogonal transformations matrices (depending on the dipole which is selected) should be used in calculation of J_{eff} .

Finite size behavior of J_{eff} is also analyzed. Variation of J_{eff} with lattice size follows the asymptotic behavior as $L \rightarrow \infty$, which is shown by the solid line in Fig. 9. In this figure $J_{\text{eff}}(\infty)$ extrapolated at the intersection of solid line and vertical axis. Line intercept corresponds to $\vec{\mathbf{J}}_{\text{eff}}(\infty) \approx$

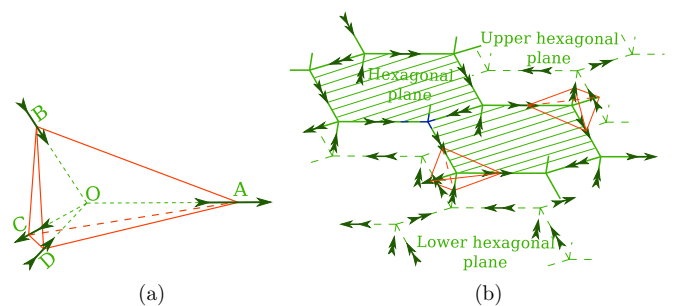


FIG. 8. (a) Dark arrows (\rightarrow) placed on the tetrahedron's vertices A, B, C, and D are shown dipoles. They are aligned to OA, BO, OC, and DO, respectively, where O shows the tetrahedron's center. (b) Stack of honeycomb structures. The diagonal hatch pattern (///) marks a mediate hexagonal plane. Unlike to what is seen from the appearance of the figure the hexagonal planes are not flat. Each plane corresponds to hexagonal sublattices A and B. For simplicity, only two of tetrahedrons have been shown here. One from the sublattice A that creates a connection to an upper plane and another from sublattice B that connects hexagonal plane to a lower plane.

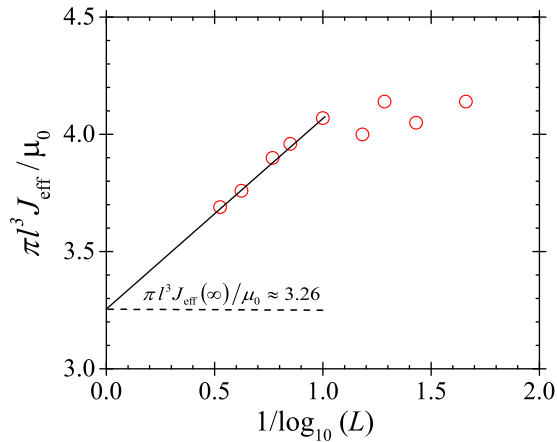


FIG. 9. $J_{\text{eff}}(L)$ plotted in terms of $1/\log_{10}(L)$, where $2L$ shows the lattice size. Solid line shows the linear fit to the data points. $\lim_{L \rightarrow \infty} J_{\text{eff}}(L)$ corresponds to a linear interception $\approx 3.26\mu_0/(\pi l^3)$ on the vertical axis.

$3.26\mu_0/(\pi l^3)\mathbb{1}$. Thus, the method of Sec. II, explained in detail from Eqs. (9) to (13), can be used to estimate the value of $\lambda_c^{(3D)} \approx 0.91$. The value obtained from the mean-field theory is the same as the corresponding dimensionless number obtained for a system of electric dipoles with dipole-dipole interaction in ice I_h . Here, we ignore the native frustration well known and understood in the ice I_h lattice and to calculate the critical condition, we do not perform the averaging over all configurations. If frustration is taken into account the system would have many states with similar minimum value of energy with strong effects on the so-called residual entropy,

but it would have little effect on the accuracy of average effective interaction energy in ground state.

APPENDIX C: ESTIMATING BIOLOGICAL PARAMETERS

Based on the experiments performed by Kirschvink *et al.*, brain tissue contains some five million magnetic nanoparticles per gram, which are organized in about 5×10^4 superclusters per gram. But the density of superclusters in the human brain meninges is about 20 times that of the brain tissue [2].

The volume number density of superclusters in the meninges $\rho^{(m)}$ is $1 \times 10^3 / \text{mm}^3$, so the average center-to-center distance of superclusters in meninges tissue is $l_{\text{sc}}^{(m)} \sim 1. \times 10^2 \mu\text{m}$ [2]. This value is about three times smaller than the same distance in the neocortex tissue, i.e., $l_{\text{sc}}^{(\text{nc})} \sim 3 \times 10^2 \mu\text{m}$.

Magnetic moment, $\mu \approx N_{\text{sc}}\mu_m$ is the approximate net dipole moment of the superclusters where N_{sc} stands for the number of SD particles in a supercluster ~ 100 and μ_m is the average magnetic dipole moment of a SD nanoparticle. μ_m is proportional to the SD nanoparticle volume, so $\langle \mu_m \rangle_a \propto \langle a^3 \rangle_a$, where $\langle \dots \rangle_a$ shows the average over the distribution of particles. Kirschvink *et al.*, estimate the size distribution of SD nanoparticle to be bimodal, though the sample size is not large. One can estimate the probability density function by using the combination of two log-normal distributions and estimate $\langle a^3 \rangle_a^{1/3} \approx 85 \text{ nm}$, which is not equal to $\langle a \rangle_a = \bar{a} \approx 50 \text{ nm}$, because the positive tail of distribution has more significant contribution to higher order moments. We use $\bar{\mu}_m \sim 1.4 \times 10^{-15} \text{ Am}^2$ for a typical nanoparticle with radius $\sim 85 \text{ nm}$ which is slightly smaller than the particle size considered in the literature ($\bar{a} \sim 100 \text{ nm}$ and $\bar{\mu}_m \sim 2.24 \times 10^{-15} \text{ Am}^2$ [45]). Thus, the acceptable value for $\bar{\mu}_m$ is in the range of $1.4\text{--}2.2 \times 10^{-15} \text{ Am}^2$.

- [1] L. Alonso-Nanclares, J. Gonzalez-Soriano, J. Rodriguez, and J. DeFelipe, *Proc. Natl. Acad. Sci. USA* **105**, 14615 (2008).
- [2] J. L. Kirschvink, A. Kobayashi-Kirschvink, and B. J. Woodford, *Proc. Natl. Acad. Sci. USA* **89**, 7683 (1992).
- [3] V. Binhi, *Int. J. Radiat. Biol.* **84**, 569 (2008); I. Bókkon and V. Salari, *J. Biol. Phys.* **36**, 109 (2010); E. P. Raven, P. H. Lu, T. A. Tishler, P. Heydari, and G. Bartzokis, *J. Alzheimers Dis.* **37**, 127 (2013); D. A. Kuterbach and B. Walcott, *J. Exp. Biol.* **126**, 375 (1986); M. A. M. Banaclocha, I. Bókkon, and H. M. Banaclocha, *Med. hypotheses* **74**, 254 (2010); P. Zuddas, D. Faivre, and J. Duhamel, in *Medical Geochemistry*, edited by P. Censi, T. H. Darrah, and Y. Erel (Springer, Berlin, 2013), pp. 91–99.
- [4] A. E. Cohen, *J. Phys. Chem. A* **113**, 11084 (2009).
- [5] E. Hand, *Science* **352**, 1508 (2016).
- [6] S. Johnsen and K. J. Lohmann, *Nat. Rev. Neurosci.* **6**, 703 (2005).
- [7] J. L. Kirschvink, D. S. Jones, and B. J. MacFadden (eds.), *Magnetite Biomineralization and Magnetoreception in Organisms: A New Biomagnetism* (Plenum Press, London, 1985), Vol. 5; S. Johnsen and K. J. Lohmann, *Phys. Today* **61**, 29 (2008); K. J. Lohmann, *Nature* **464**, 1140 (2010).
- [8] M. M. Walker, T. E. Dennis, and J. L. Kirschvink, *Curr. Opin. Neurobiol.* **12**, 735 (2002); L. C. Boles and K. J. Lohmann, *Nature* **421**, 60 (2003); K. J. Lohmann, C. M. Lohmann, and N. F. Putman, *J. Exp. Biol.* **210**, 3697 (2007).
- [9] F. Brown, H. Webb, and W. Brett, *Biol. Bull.* **118**, 382 (1960); V. L. Bliss and F. H. Heppner, *Nature* **261**, 411 (1976).
- [10] R. K. Adair, *Phys. Rev. A* **43**, 1039 (1991).
- [11] J. L. Kirschvink, *Phys. Rev. A* **46**, 2178 (1992).
- [12] J. L. Kirschvink and J. L. Gould, *Biosystems* **13**, 181 (1981).
- [13] V. P. Shcherbakov and M. Winklhofer, *Eur. Biophys. J* **28**, 380 (1999); A. Davila, G. Fleissner, M. Winklhofer, and N. Petersen, *Phys. Chem. Earth* **28**, 647 (2003); S. Krichen, L. Liu, and P. Sharma, *Phys. Rev. E* **96**, 042404 (2017).
- [14] D. Faivre and D. Schuler, *Chem. Rev.* **108**, 4875 (2008).
- [15] H. Stanjek, J. Fassbinder, H. Vali, H. Wägele, and W. Graf, *Eur. J. Soil. Sci.* **45**, 97 (1994).
- [16] M. M. Walker, T. P. Quinn, J. L. Kirschvink, and C. Groot, *J. Exp. Biol.* **140**, 51 (1988).
- [17] J. L. Gould, J. Kirschvink, and K. Deffeyes, *Science* **201**, 1026 (1978); C.-Y. Hsu, F.-Y. Ko, C.-W. Li, K. Fann, and J.-T. Lue, *PLoS one* **2**, e395 (2007); C.-H. Liang, C.-L. Chuang, J.-A. Jiang, and E.-C. Yang, *Sci. Rep.* **6**, 23657 (2016).

- [18] F. T. De Araujo, M. Pires, R. B. Frankel, and C. Bicudo, *Biophys. J.* **50**, 375 (1986).
- [19] G. Fleissner, B. Stahl, P. Thalau, G. Falkenberg, and G. Fleissner, *Naturwissenschaften* **94**, 631 (2007); G. Fleissner, G. Fleissner, B. Stahl, and G. Falkenberg, *J. Field Ornithol.* **148**, 643 (2007).
- [20] R. Blakemore, *Science* **190**, 377 (1975).
- [21] C. D. Treiber, M. C. Salzer, J. Riegler, N. Edelman, C. Sugar, M. Breuss, P. Pichler, H. Cadiou, M. Saunders, M. Lythgoe *et al.*, *Nature* **484**, 367 (2012); H. Mouritsen, *ibid.* **484**, 320 (2012); in *Sturkie's Avian Physiology*, edited by C. Scanes (Academic Press, San Diego, CA, 2015), pp. 113–133; D. Kishkinev and N. Chernetsov, *Biol. Bull. Rev.* **5**, 46 (2015).
- [22] J. L. Kirschvink, A. Kobayashi-Kirschvink, J. C. Diaz-Ricci, and S. J. Kirschvink, *Bioelectromagnetics* **13**, 101 (1992).
- [23] B. A. Maher, I. A. Ahmed, V. Karloukovski, D. A. MacLaren, P. G. Foulds, D. Allsop, D. M. Mann, R. Torres-Jardón, and L. Calderon-Garciduenas, *Proc. Natl. Acad. Sci. USA* **113**, 10797 (2016).
- [24] R. Gieré, *Proc. Natl. Acad. Sci. USA* **113**, 11986 (2016), see also S. A. Gilder, M. Wack, L. Kaub, S. C. Roud, N. Petersen, H. Heinsen, P. Hillenbrand, S. Milz, and C. Schmitz, *Sci. Rep.* **8**, 11363 (2018).
- [25] F. Brem, L. Tiefenauer, A. Fink, J. Dobson, and A. M. Hirt, *Phys. Rev. B* **73**, 224427 (2006).
- [26] I. Goychuk, *Phys. Rev. E* **92**, 042711 (2015); M. Winklhofer and J. L. Kirschvink, *J. R. Soc. Interface* **7**, S273 (2010); V. P. Shcherbakov and M. Winklhofer, *Phys. Rev. E* **81**, 031921 (2010).
- [27] H. Zhang and M. Widom, *Phys. Rev. E* **49**, R3591 (1994).
- [28] H. Zhang and M. Widom, *J. Magn. Magn. Mater.* **122**, 119 (1993).
- [29] J. M. Luttinger and L. Tisza, *Phys. Rev.* **70**, 954 (1946); **72**, 257 (1946).
- [30] M. S. Wertheim, *J. Chem. Phys.* **55**, 4291 (1971).
- [31] B. E. Vugmeister and M. D. Glinchuk, *Rev. Mod. Phys.* **62**, 993 (1990).
- [32] B. Huke and M. Lücke, *Rep. Prog. Phys.* **67**, 1731 (2004).
- [33] H. Mamiya, I. Nakatani, and T. Furubayashi, *Phys. Rev. Lett.* **84**, 6106 (2000).
- [34] M. A. M. Banaclocha, *Brain Res. Bull.* **73**, 21 (2007).
- [35] J. Howard and A. Hudspeth, *Neuron* **1**, 189 (1988).
- [36] W. T. Coffey, Y. P. Kalmykov, and J. T. Waldron, *The Langevin Equation with Applications to Stochastic Problems in Physics, Chemistry and Electrical Engineering*, 2nd ed., in Contemporary Chemical Physics Series, Vol. 14 (World Scientific, Singapore, 2004).
- [37] C. Morris, J. Candy, A. Oakley, C. Bloxham, and J. Edwardson, *Cells Tissues Organs* **144**, 235 (1992); M. Kopáni, J. Hlinková, H. Ehrlich, D. Valigura, and R. Boča, *J. Bioanal. Biomed.* **9**, 080 (2017).
- [38] H. Paganetti, H. Jiang, J. A. Adams, G. T. Chen, and E. Rietzel, *Int. J. Radiat. Oncol.* **60**, 942 (2004).
- [39] D. Fraiman, P. Balenzuela, J. Foss, and D. R. Chialvo, *Phys. Rev. E* **79**, 061922 (2009).
- [40] M. G. Paulin, *J. Theor. Biol.* **174**, 325 (1995).
- [41] J. Cardy, *Scaling and Renormalization in Statistical Physics* (Cambridge University Press, Cambridge, 1996).
- [42] J. Dobson, *Exp. Brain Res.* **144**, 122 (2002).
- [43] F. Brem, A. M. Hirt, M. Winklhofer, K. Frei, Y. Yonekawa, H.-G. Wieser, and J. Dobson, *J. R. Soc. Interface* **3**, 833 (2006).
- [44] L. Pauling, *J. Am. Chem. Soc.* **57**, 2680 (1935).
- [45] O. Strbak, P. Kopcansky, and I. Frollo, *Meas. Sci. Rev.* **11**, 85 (2011); T. E. Vaughan and J. C. Weaver, *Biophys. J.* **71**, 616 (1996).